Scientia Pharmaceutica

ÖSTERREICHISCHE PHARMAZEUTISCHE GESELLSCHAFT

MDPI

Article

Phytochemical Characterization of *Pterocephalus frutescens* with In-Silico Evaluation as Chemotherapeutic Medicine and Oral Pharmacokinetics Prediction Study

Atef A. El-Hela [1], Marwa S. Abu Bakr [2], Mostafa M. Hegazy [1], Mohammed A. Dahab [3], Ayman Abo Elmaaty [4], Adel Ehab Ibrahim [5,6], Sami El Deeb [5,7,*] and Hatem S. Abbass [1,8]

1 Department of Pharmacognosy and Medicinal Plants, Faculty of Pharmacy, Al-Azhar University (Boys), Cairo 11884, Egypt
2 Department of Pharmacognosy and Medicinal Plants, Faculty of Pharmacy, Al-Azhar University (Girls), Cairo 11884, Egypt
3 Department of Pharmaceutical Medicinal Chemistry & Drug Design, Faculty of Pharmacy, Al-Azhar University (Boys), Cairo 11884, Egypt
4 Department of Medicinal Chemistry, Faculty of Pharmacy, Port-Said University, Port-Said 42526, Egypt
5 Natural and Medical Sciences Research Center, University of Nizwa, P.O. Box 33, Birkat Al Mauz, Nizwa 616, Oman
6 Department of Pharmaceutical Analytical Chemistry, Faculty of Pharmacy, Port-Said University, Port-Said 42526, Egypt
7 Institute of Medicinal and Pharmaceutical Chemistry, Technische Universitaet Braunschweig, 38092 Braunschweig, Germany
8 Department of Pharmacognosy, Faculty of Pharmacy, Sinai University—Kantara Branch, Ismailia 41636, Egypt
* Correspondence: s.eldeeb@tu-braunschweig.de

Abstract: Virtual screening of the potential lead chemotherapeutic phytochemicals from medicinal plants has useful application in the field of in-silico modelling and computer-based drug design by orienting and scoring ligands in the active binding site of a target protein. The phytochemical investigation of the *Pterocephalus frutescens* extract in n-butanol resulted in the isolation and structure elucidation of three iridoids and four flavonoids which were identified as Geniposide (**1**), Geniposidic acid (**2**), Nepetanudoside C (**3**), Isovitexin (**4**), Luteolin-7-O-glucoside (**5**) Isoorientin (**6**) and Orientin (**7**), respectively. Molecular docking studies were used to compare the binding energies of the isolated phytochemicals at four biological cancer-relevant targets; namely, aromatase, carbonic anhydrase IX, fatty acid synthase, and topoisomerase II-DNA complex. The docking study concluded that the isolated compounds have promising cytotoxic activities, in particular, Luteolin-7-O-glucoside (**5**) and Orientin (**7**) which exhibited high binding affinities among the isolated compounds at the active sites of the target enzymes; Aromatase (−8.73 Kcal/mol), and Carbonic anhydrase IX (−8.92 Kcal/mol), respectively, surpassing the corresponding binding scores of the co-crystallized ligands and the reference drugs at these target enzymes. Additionally, among the isolated compounds, Luteolin-7-O-glucoside (**5**) showed the most outstanding binding affinities at the active sites of the target enzymes; Fatty acid synthase, and Topisomerase II-DNA complex with binding scores of −6.82, and −7.99 Kcal/mol, respectively. Finally, the SwissADME online web tool predicted that most of these compounds possessed acceptable oral bioavailability and drug likeness characteristics.

Keywords: drug likeness; Lipinski's rule; molecular docking; pterocephalus frutescens; chemical profiling; phytochemicals

Citation: El-Hela, A.A.; Bakr, M.S.A.; Hegazy, M.M.; Dahab, M.A.; Elmaaty, A.A.; Ibrahim, A.E.; El Deeb, S.; Abbass, H.S. Phytochemical Characterization of *Pterocephalus frutescens* with In-Silico Evaluation as Chemotherapeutic Medicine and Oral Pharmacokinetics Prediction Study. *Sci. Pharm.* **2023**, *91*, 7. https://doi.org/10.3390/scipharm91010007

Academic Editor: Roman B. Lesyk

Received: 27 December 2022
Revised: 23 January 2023
Accepted: 26 January 2023
Published: 28 January 2023

1. Introduction

The family Caprifoliaceae consists of 42 genera and approximately 860 species, which are distributed mainly in Europe, Asia and Africa. Some members of this family have been

transferred and naturalized in different places [1]. The Pterocephalus genus comprises 25 species which are widely used in traditional medicine around the entire globe for their antibacterial, anti-inflammatory, antioxidant, antihepatotoxic, and analgesic activities [2–5]. Many phytochemicals that contribute to the biological activities of the genus Pterocephalus are natural products that have been isolated and include flavonoids, iridoids, phenolic acids, saponins and lignans [6–9]. Meanwhile, chemotherapy can be considered one of the most important approaches for the treatment of cancer, and therefore, potential chemotherapeutic targets for cancer are being identified [10,11]. The use of phytochemicals in the treatment of cancer has been widely reported. For instance, vincristine and paclitaxel are the phytochemicals that have been clinically used as the chemotherapeutic agents [12]. Flavonoids are another class of the phytochemicals that have demonstrated promising chemotherapeutic and cancer preventive activities, in addition to other anti-inflammatory effects [13,14].

Several biological molecules had been investigated as targeted therapy for treatment of different types of cancer. Targeted therapy aims at selecting specific proteins that share in the proliferation and growth of cancer, and hence chemotherapeutic agents can stop the spread of cancer. Among those biological targets, aromatase, carbonic anhydrase IX, fatty acid synthase, and topoisomerase II-DNA complex have gained attention. Aromatase is an important enzyme for the biosynthesis of estrogens, which catalyzes the transformation of androgen by aromatization. Estrogens, in turn, were identified to play a crucial role in breast cancer development [15]. Aromatase has also been recently studied for multi-targeted chemotherapy [16,17]. Some phytochemical agents, such as rotenone, chrysin and apigenin flavonoids, have been reported to potently inhibit the aromatase cytochrome p450 enzyme [18]. On the other hand, the fatty acid synthase (FAS) is the major enzyme in the biosynthesis of different fatty acids. FAS has been shown to be expressed in high levels in many tumor cancers [19]. Consequently, they can provide flexibility in energy supply, especially to the lipogenic phenotype tumors [20]. As such, the FAS has been an attractive target where certain phytochemical flavonoids were studied to show a dose-response correlation between FAS and apoptosis induction in tumor cells [21].

Another major group of biological targets are the topoisomerases, which are essential enzymes catalyzing the modifications in the tertiary structure of the DNA. There are two classes of human topoisomerases (I and II). Topoisomerase II (the ATP binding site) involves double-strand breaking [22]. The topoisomerases have been widely studied as antimicrobial and anticancer targets [23]. A recent study, by Han et al. [24], confirmed the importance of topoisomerase inhibitors as anti-cancer remedies, however, the main obstacle was their off-target toxicity. The use of naturally derived phytochemicals, such as podophyllotoxin, anthracycline, genistein and camptothecin has been investigated for different types of tumors by inhibiting both topoisomerase I and II [25,26]. Another important player in tumor development and proliferation is the carbonic anhydrase IX (CAIX), which is induced by the regional hypoxia and acidosis created within the cancer cells. This enzyme helps the mutant cells in withstanding the hostile micro-environment created and therefore allows them to selectively proliferate and progress [27]. Therefore, several studies have been conducted investigating the effect of the CAIX inhibitors in the control of tumors [28,29].

The present work aimed at identifying the major phytoconstituents in the plant material, *P. frutescens*, using isolation and structure elucidation. Another in-silico study for the isolated phytochemicals was carried out to investigate their possible utility as chemotherapeutic agents using molecular docking through examining their potential binding to cancer-relevant molecular targets, namely aromatase, carbonic anhydrase IX, fatty acid synthase, and topoisomerase II-DNA complex. Finally, to verify that these compounds are promising candidates from the aspect of pharmacokinetics, the SwissADME online web tool developed by the molecular modelling group of Swiss Institute of Bioinformatics (SIB) was used to compute the physicochemical properties and predict the pharmacokinetic and the drug likeness properties of our target compounds [30].

2. Experimental Design

2.1. Plant Material

The aerial parts of *P. frutescens* Hochist. were collected in June 2017 at the flowering stage from the from Jabal An-NabiShu'ahyb, Sanaa, Republic of **Yemen**. The plants were collected, identified and authenticated by Dr. Abdo H. Marey Professor of Botany and Plant Taxonomy, Faculty of Science, Al-Azhar University, Cairo Egypt. A voucher sample was kept in the Herbarium of Faculty of Pharmacy, Al-Azhar University. Cairo, Egypt.

2.2. Extraction and Isolation of Pure Compounds

Air-dried powdered aerial part plant material of *P. frutescens* (250 g), was extracted by a soxhlet apparatus with n-hexane (2 × 2 L) and then with methanol (3 × 3 L) to afford (7.5 and 35 g, respectively) after evaporation under vacuum by rotatory evaporator (BUCHI Rotavapor® R-210/R-215, Labfirst Scientific, CA, USA). From the methanol extract 35 g was dissolved in water and then partitioned successively with ethyl acetate (2 × 200 mL) and *n*-butanol saturated with water (3 × 200 mL) to afford light brown masses (8.5 and 11 g, respectively). The *n*-butanol fraction (11 g) was separated on polyamide (200 g) using stepwise gradient elution with water: methanol (100:0–0:100) to yield 4 fractions. Fraction 2 (1.8 g) was re chromatographed on silica gel (40 g) by gradient elution with chloroform: methanol: water (90:10:1) to yield 3 sub fractions. Sub fraction 2 (360 mg) was chromatographed on silica gel and eluted with chloroform: methanol (90:10) then (85:15) to yield 5 sub fractions. Sub fraction 2.1, 2.4 and 2.5 (50, 60 and 40 mg, respectively) were purified individually by sephadex LH_{20} (50 g) with methanol to give compounds (**1**, **2** and **3**) (22, 38 and 30 mg, respectively). Fraction 3 (2.3 g) was re chromatographed on silica gel (80 g) by isocratic elution with benzene: methanol: water (100:50:3) to give 5 sub fractions. Sub fraction 3.5 (500 mg) was re chromatographed by Sephadex LH_{20} (100 g) with methanol to give compound (**4**) (25 mg). Fraction 4 (1.9 g) was re chromatographed on reversed phase (RP) solid phase extraction (SPE) (50 g) by gradient elution with water: methanol (90:10–10:90) to give 4 sub fractions. Sub fraction 4.1 (280 mg) was purified by Sephadex LH_{20} (100 g) by isocratic elution with methanol to give compound (**5**) (15 mg). Sub fraction 4.2 (200 mg) and 4.3 (340 mg) were purified individually by Sephadex LH_{20} (100 g) by isocratic elution with methanol: chloroform (60:40) to give compound (**6**) (14 mg) and compound (**7**) (32 mg).

2.3. Structure Elucidation of Isolated Pure Compounds

Nuclear magnetic resonance (NMR) spectra were obtained using a Bruker spectrometer (Rheinstetten, Karlsruhe, Germany). Deuterated methanol (CD_3OD) and dimethyl sulfoxide (DMSO-d_6) were used as solvents.

2.4. Molecular Docking Analysis

The anticancer activities of the afforded compounds were investigated against four relevant biological targets namely; aromatase enzyme, carbonic anhydrase IV, fatty acid synthase, and topoisomerasr II-DNA complex using Autodock program.

2.4.1. Preparation of the Investigated Compounds

The investigated compounds were chemically sketched by ChemBioDraw Ultra 14.0 (Figure 1) to be ready for the docking process as previously described [31–38]. For each biological target, the afforded compounds were imported into one database saving it as an MDB extension file.

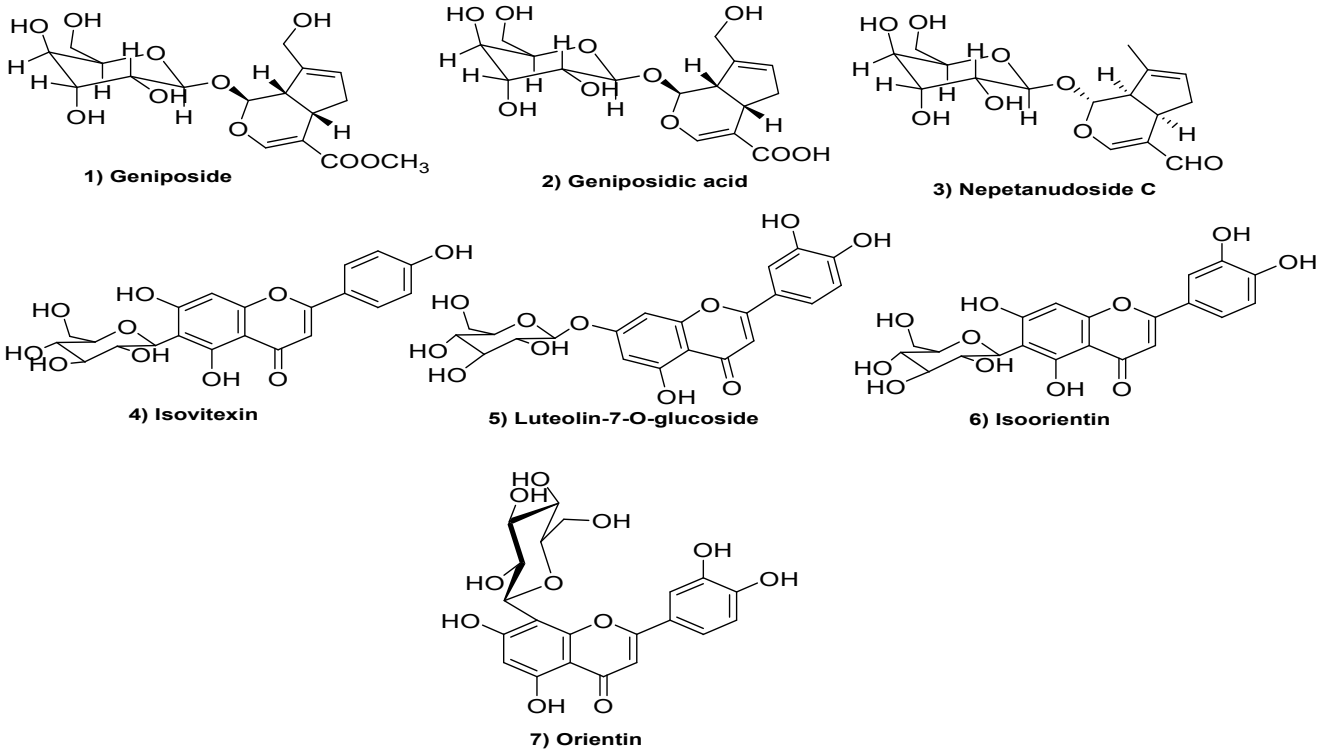

Figure 1. Structures of flavonoids and iridoids isolated from P. frutescens Hochist.

2.4.2. Preparation of Helicobacter Specific Virulence Proteins

The X-ray structure of the determined biological targets was selected carefully and downloaded from the online protein data bank website. The PDB entries for aromatase enzyme, CA IV, FAS, and TOP II were, 5jl9 [39], 5fl4 [40], 2px6 [41], and 3qx3 [42], respectively. Subsequently, the biological target proteins were protonated, and broken bonds were corrected, followed by biological protein energy minimization in order to be ready for the established docking process as previously mentioned in detail [31].

3. Results and Discussion

3.1. Strutural Elucidation of Isolated Pure Compounds

Compound (**1**) was obtained as white crystals with ESIMS *m/z*: 387 $[M-H]^-$; (calculated for $C_{17}H_{24}O_{10}$). ^{1}H NMR (CD_3OD, 400 MHz) δ 5.19 (1H, d, *J* = 7.5 Hz, H-1) 7.53 (1H, s, H-3); 3.22 (1H, overlap, H-5); 2.13 (1H, m, H-6a); 2.84 (1H, dd, *J* = 8.0, 16.0Hz, H-6b); 5.82 (1H, s, H-7); 2.74 (1H, t, *J* = 7.5 Hz, H-9); 4.20 (1H, d, *J* = 14.5 Hz, H-10a); 4.33 (1H, d, *J* = 14.5 Hz, H-10b); 3.73 (3H, s, H-12); 4.73 (1H, d, *J* = 7.5 Hz, H-1′); 3.23–3.41 (4H, m, H-2′, 3′, 4′, 5′); 3.65 (1H, dd, *J* = 4.0, 9.5 Hz, H-6a′); 3.88 (1H, brd, *J* = 12.0 Hz, H-6b′). ^{13}C-NMR (CD_3OD, 100 MHz) δ 100.2 (C-1); 155.3 (C-3); 114.5 (C-4); 38.6 (C-5); 41.8 (C-6); 130.3 (C-7); 146.9 (C-8); 49.1 (C-9); 63.5 (C-10); 171.6 (C-11); 53.8 (C-12); 102.4 (C-1′); 76.9 (C-2′); 80.0 (C-3′); 73.7 (C-4′); 80.6 (C-5′); 63.7 (C-6′). From the above data compound (**1**) was identified as Geniposide [43].

Compound (**2**) was obtained as an amorphous powder with ESIMS *m\z*: 363 $[M-H]^-$; (calculated for $C_{16}H_{22}O_{10}$). ^{1}H NMR (CD_3OD, 400 MHz) δ 5.11 (1H, *d*, *J* = 7.5 Hz, H-1), 7.31 (1H, s, H-3), 3.23 (1H, *m*,H-5), 2.09 (1H, *dd*, *J* = 16.2/7.6 Hz, H*a*-6), 2.86 (1H, *dd*, *J* = 16.2/7.6 Hz, H*b*-6), 5.79 (1H, *brs*, H-7), 2.70(1H, *t*, *J* = 7.5 Hz, H-9), 4.18 (1H, *d*, *J* = 14.6 Hz, H*a*-10), 4.33 (1H, *d*, *J* = 14.3 Hz, H*b*-10), 4.74 (1H, *d*, *J*= 7.6 Hz, H-1′), 3.18–3.45 (4H, *m*, H-2′, H-3′, H-4′, H-5′), 3.69 (1H, *dd*, *J* = 11.9/5.5 Hz, H*a*-6′), 3.85 (1H, *dd*, *J* = 11.6/1.7 Hz, H*b*-6′). ^{13}C-NMR (CD_3OD, 100 MHz) δ 98.2 (C-1), 153.2 (C-3), 112.8 (C-4), 36.7 (C-5), 39.7 (C-6), 127.8 (C-7), 143.3 (C-8), 47.0 (C-9), 61.4 (C-10), 173.0 (C-11), 100.3 (C-1), 74.8 (C-2), 77.4

(C-3), 71.5 (C-4), 78.8 (C-5), 62.6 (C-6). From the above data compound (**2**) was identified as Geniposidic acid [43].

Compound (**3**) was obtained as an amorphous powder with ESIMS *m*\z: 341 $[M-H]^-$; (calculated for $C_{16}H_{22}O_8$). ^{1}H NMR (CD_3OD, 400 MHz) δ 5.40 (d, 4.6, H-1), 7.34 (s, H-3), 3.13 (m, H-5), 2.18 (m, H-6), 2.76 (m, H-6), 5.49 (m, H-7), 2. 91(m, H-9), 1.82 (br s, H3-10), 9.21 (s, H-11), 4.64(d, 7.6, H-1′), 3.69 (dd, 12.0, 3.8, H-6a′), 3.87 (br d, 12.0, H-6b′); 3.22–3.42 (4H, *m*, H-2′, H-3′, H-4′, H-5′). ^{13}C-NMR (CD_3OD, 100 MHz) δ 101.4 (C-1), 158.8 (C-3), 121.6 (C-4), 32.8 (C-5), 38.5 (C-6), 128.2 (C-7), 139.5 (C-8), 50.45 (C-9), 15.3 (C-10), 193.4 (C-11), 103.8 (C-1), 75.5 (C-2), 78.7 (C-3), 71.5 (C-4), 78.4 (C-5), 62.2 (C-6). From the above data compound (**3**) was identified as Nepetanudoside C [44].

Compound (**4**) was obtained as a yellow powder with ESIMS *m*\z: 431 $[M-H]^-$; (calculated for $C_{21}H_{20}O_{10}$). ^{1}H NMR (DMSO-d_6, 400 MHz) δ 13.48 (1H, brs, 5-OH), 7.79 (2H, d, *J* = 8.3 Hz, 3′, 5′-H), 6.89 (2H, d, *J* = 8.2 Hz, 2′, 6′-H), 6.70(1H, s, 3-H), 6.39 (1H, s, 8-H), 4.51 (1H, d, *J* = 9.7 Hz, 1″-H). 3.40–3.95 (sugar protons, *m*). ^{13}C-NMR (DMSO-d_6, 100 MHz) δ 163.71 (C-2), 102.90(C-3), 181.83 (C-4), 160.52 (C-5), 108.82 (C-6), 163.55 (C-7), 93.94 (C-8), 155.91 (C-9), 102.76 (C-10), 121.24 (C-1′), 128.65 (C-2′, 6′), 115.89 (C-3′, 5′), 161.46 (C-4′), 73.55 (C-1″), 70.86 (C-2″)), 79.03 (C-3″)), 70.43 (C-4″), 81.53 (C-5″), 61.42 (C-6″). From the above data compound (**4**) was identified as Isovitexin [45].

Compound (**5**) was obtained as a yellow crystalline powder, with ESIMS *m*\z: 447 $[M-H]^-$; (calculated for $C_{21}H_{20}O_{11}$). ^{1}H NMR (DMSO-d_6, 400 MHz) 13.13 (1H, s, 5-OH), 7.49 (1H, dd, *J* = 2.2, 8.2 Hz, H-6′), 7.43 (1H, d, *J* = 2.2 Hz, H-2′), 6.91 (1H, d, *J* = 8.2 Hz, H-5′), 6.68 (1H, s, H-3), 6.32(1H, s, H-6), 4.67 (1H, d, *J* = 9.3 Hz, H-1′′), 3.30–3.90 (sugar protons, *m*). ^{13}C-NMR (DMSO-d_6, 100 MHz) δ 164.32(C-2), 102.75 (C-3), 182.32 (C-4), 160.76 (C-5), 98.32 (C-6), 162.96 (C-7), 105.05 (C-8), 156.60 (C-9), 104.30(C-10), 122.11 (C-1′), 114.57 (C-2′), 146.15 (C-3′), 150.20 (C-4′), 115.88 (C-5′), 119.64 (C-6′), 73.67 (C-1″),70.99 (C-2″), 78.97 (C-3″), 70.93 (C-4″), 82.20 (C-5″), 61.96 (C-6″). From the above data compound (**5**) was identified as Orientin [46].

Compound (**6**) was obtained as a yellow powder, with ESIMS *m*\z: 447 $[M-H]^-$; (calculated for $C_{21}H_{20}O_{11}$). ^{1}H NMR (DMSO-d_6, 400 MHz) δ 13.53 (1H, brs, 5-OH), 7.42 (1H, dd, *J* = 2.4 Hz, 9.0 Hz, 6′-H), 7.36 (1H, d, *J* = 2.4 Hz, 2′-H), 6.90 (1H, d, *J* = 9.0 Hz, 5′-H), 6.64 (1H, S, 3-H), 6.48(1H, s, H-8), 4.58 (1H, d, *J* = 10.0 Hz, 1′′-H). 3.30–3.90 (sugar protons, *m*). ^{13}C-NMR (DMSO-d_6, 100 MHz) δ 163.65 (C-2), 102.76 (C-3), 181.86 (C-4), 160.91 (C-5), 108.95 (C-6), 163.78 (C-7), 94.04 (C-8), 156.75 (C-9), 102.91 (C-10), 121.86 (C-1′), 113.32 (C-2′), 146.34 (C-3′), 150.73 (C-4′), 116.53 (C-5′), 119.21 (C-6′), 73.42 (C-1″)),70.53 (C-2″)), 79.23 (C-3″), 70.43 (C-4″), 81.78 (C-5″), 61.68 (C-6″). From the above data compound (**6**) was identified as Isoorientin [46].

Compound (**7**) was obtained as a yellow microcrystalline powder with ESIMS *m*\z: 447 $[M-H]^-$; (calculated for $C_{21}H_{20}O_{11}$). ^{1}H NMR (DMSO-d_6, 400 MHz) δ 6.54 (1H, *d*, *J* = 1.5 Hz, H-6), 6.84 (1H, *s*,H-3), 6.87 (1H, *d*, *J* = 1.5 Hz, H-8), 6.85 (1H, *d*, *J* =8.1 Hz, H-5′), 7.55 (2H, *d*, *J* = 8 Hz, H-2′,6′). 5.01 (1H, *d*, *J* = 7.5 Hz, H-1″), 4.36 (1H, *d*, *J*_12.8 Hz, H-6″a), 4.15 (2H, *m*, H-3″, H-6″b), 4.08 (1H, *m*, H-2″), 4.02 (2H, *m*, H-4″, H-5″). ^{13}C-NMR (DMSO-d_6, 100 MHz) δ 61.65 (C-6″), 70.76 (C-4″), 73.92 (C-2″), 77.35 (C-3″), 78.00 (C-5″),95.76 (C-8), 100.36 (C-6), 100.87 (C-1″), 103.95(C-3), 106.43 (C-10), 114.43 (C-2′), 116.84 (C-5′),119.98 (C-6′), 121.89 (C-1′), 146.74 (C-3′), 151.53(C-4′), 157.74 (C-9), 162.05 (C-5), 163.90 (C-2),165.53 (C-7), 182.84 (C-4). From the above data compound (**7**) was identified as Luteolin-7-O-glucoside (cynaroside) [47].

3.2. Results of In Silico Studies

Molecular Docking Analysis

The conducted molecular docking studies were employed to investigate the binding affinities of Geniposide (**1**), Geniposidic acid (**2**), Nepetanudoside C (**3**), Isovitexin (**4**), Luteolin-7-O-glucoside (**5**) Isoorientin (**6**) and Orientin (**7**) towards the biological targets; aromatase, carbonic anhydrase IX, fatty acid synthase, and topoisomerase II-DNA complex. First, prescreening validation was carried out to emphasize the accuracy of the utilized

Autodock docking program. Hence, the validation process was carried out by the re-docking of the co-crystallized ligand for each target receptor. Obviously, low RMSD values were attained (1.84, 1.72, 1.88, and 1.42 Å for aromatase, carbonic anhydrase IX, fatty acid synthase, and topoisomerase II-DNA complex, respectively) assuring the employed program's validity [32,48–52]. The 2D and 3D overlay of the native co-crystallized ligands and the re-docked co-crystallized ligands were illustrated in the supplementary Figures S1–S4. Hence, the molecular docking was conducted to afford further insights about the investigated compounds' binding modes on these target proteins, thus unveiling their potential as new eligible anticancer candidates. The binding free energy scores, RMSD, and the binding interactions for the investigated compounds are depicted in Tables 1 and 2.

Table 1. Binding scores, RMSD values, and amino acid binding interactions of the investigated compounds against aromatase and carbonic anhydrase IX.

Aromatase Enzyme					CA IX				
Comp. No	**S Score (Kcal/mol)**	**RMSD (Å)**	**Binding Interaction**	**Distance (Å)**	**Comp. No**	**S Score (Kcal/mol)**	**RMSD (Å)**	**Binding Interaction**	**Distance (Å)**
(1)	−8.15	0.70	LEU372/H-donor MET374/H-acceptor	2.93 3.10	**(1)**	−7.41	1.43	GLU106/H-donor THR200/H-acceptor	3.14 3.07
(2)	−7.70	0.89	CYS437/H-donor MET374/H-donor LEU477/H-donor	3.30 4.50 3.26	**(2)**	−7.05	1.45	THR201/H-donor THR200/H-acceptor	2.67 3.23
(3)	−7.22	1.49	LEU372/H-donor LEU477/H-donor MET374/H-acceptor ALA306/H-acceptor	3.12 2.94 3.19 3.38	**(3)**	−7.41	1.64	THR201/H-donor THR200/H-acceptor HIS94/H-pi	2.88 3.17 3.55
(4)	−8.54	2.27	LEU477/H-donor LEU477/H-donor MET374/H-acceptor ILE133/pi-H	2.83 2.72 3.37 4.22	**(4)**	−7.21	1.41	THR201/H-donor GLN71/H-acceptor ZN264/Metal LEU91/pi-H GLN92/pi-H	3.18 3.03 2.30 3.98 3.85
(5)	−8.73	1.74	MET374/H-donor LEU372/H-donor LEU477/H-donor ILE133/pi-H	3.84 2.71 3.25 4.49	**(5)**	−8.13	1.83	GLU106/H-donor	3.08
(6)	−8.52	1.27	MET303/H-donor MET303/H-donor LEU477/H-donor LEU477/H-donor MET374/H-acceptor ILE133/pi-H GLY439/pi-H	4.24 3.91 3.10 2.66 3.03 3.96 4.36	**(6)**	−7.41	1.31	ZN264/Metal	2.30
(7)	−8.67	1.81	MET374/H-donor MET374/H-acceptor	3.92 3.03	**(7)**	−8.92	2.13	THR201/H-donor	3.22
Co-crystallized	−8.02	1.84	MET374/H-acceptor	2.97	Co-crystallized	−5.91	1.72	THR201/H-donor THR200/H-acceptor VAL121/pi-H	3.27 3.34 4.93
Reference	−7.76	1.07	MET374/ H-acceptor	2.96	Reference	−5.83	1.31	THR201/H-donor THR201/H-donor THR200/H-acceptor	3.29 3.22 3.28

Table 2. Binding scores, RMSD values, and amino acid binding interactions of the investigated compounds against FAS and topoisomerase II-DNA complex.

FAS					Topisomerase II-DNA Complex				
Comp. No	**S Score**	**RMSD**	**Binding Interaction**	**Distance**	**Comp. No**	**S Score**	**RMSD**	**Binding Interaction**	**Distance**
(1)	−5.86	0.93	SER2340/H-acceptor ARG2482/H-acceptor	3.12 3.23	**(1)**	−7.31	1.77	DG10/H-donor ASP479/H-donor DT9/H-pi	2.96 2.86 3.78
(2)	−6.05	1.84	ASP2338/H-donor PRO2341/H-donor SER2340/H-acceptor TYR2462/H-pi	3.01 2.91 3.19 3.54	**(2)**	−6.87	1.46	MET782/H-donor ARG503/H-acceptor	3.16 2.99
(3)	−5.85	0.93	SER2308/H-donor THR2342/H-donor SER2340/H-acceptor HIS2481/H-pi	2.95 3.23 3.07 3.73	**(3)**	−7.16	1.44	ARG503/H-acceptor ASP479/H-acceptor DG13/H-pi DG13/H-pi	3.01 2.95 4.54 3.68
(4)	−6.22	1.09	THR2342/H-donor SER2340/H-acceptor	3.05 3.35	**(4)**	−7.47	1.15	ASP479/H-donor DT9/pi-H DT9/pi-H	3.08 4.16 4.21
(5)	−6.82	2.26	SER2340/H-donor SER2340/H-acceptor PHE2370/H-pi ILE2250/pi-H	2.97 3.02 4.53 3.80	**(5)**	−7.99	2.15	ASP479/H-donor DG10/H-donor SER480/H-acceptor DT9/pi-H	2.69 3.20 2.92 3.64
(6)	−6.49	1.10	SER2340/H-donor	3.00	**(6)**	−7.78	1.49	ASP479/H-donor DT9/H-donor	2.98 2.97
(7)	−6.40	1.61	HIS2481/H-donor	3.33	**(7)**	−7.69	2.18	ASP479/H-donor DT9/H-donor GLU477/H-donor ARG503/H-acceptor DG13/H-pi DT9/pi-H	3.00 2.71 3.03 3.11 3.66 4.47
Co-crystallized	−8.09	1.39	SER2340/H-acceptor TYR2462/H-pi HIS2481/H-pi	3.03 4.65 4.42	Co-crystallized	−10.52	1.42	ASP479/H-donor MET782/H-donor DG13/H-donor GLN778/H-acceptor DA12/H-pi	2.70 3.73 3.37 2.94 3.75
Reference	−6.03	1.76	HIS2481/pi-pi	3.92	Reference	−8.96	1.84	ARG503/H-donor ASP479/H-acceptor LYS456/H-acceptor DG13/H-pi	3.24 3.43 3.29 4.26

By analyzing the docking results obtained regarding the aromatase biological target, it was interestingly revealed that compounds (**4**, **5**, **6**, and **7**) displayed feasible binding scores surpassing that obtained by the co-crystallized ligand and the reference drug used (Exemestane). The choice of exemestane as a reference drug was based on its activity as an aromatase inhibitor, where it has a polycyclic structure which is more or less similar to the investigated compounds, so that the investigated compounds can be assured to securely bind to the selected target for a valid comparison. It worth noting that compound (**5**) revealed the most binding affinity towards the aromatase enzyme among the investigated compounds. Additionally, due to its binding to the the co-crystallized ligand and the reference drug, the amino acid MET374 could be considered as one of the pivotal amino acids for aromatase inhibition. Consequently, it was disclosed that compound (**5**) could interact with the aromatase enzyme with a binding score of −8.73 Kcal/mol with an RMSD value of 1.74 Å. Notably, the sugar moiety of compound (**5**) could form H-bonds with MET374, LEU372, and LEU477 at distances 3.84, 2.71, and 3.25 Å, respectively. In addition, the phenyl ring of compound 5 could form a pi-H bond with ILE133 at a distance of 4.49 Å.

However, the co-crystallized ligand could form an H-bond with MET374 at a distance of 2.97 Å, whereas, the reference drug used (Exemestane) could form an H-bond with MET374 at a distance of 2.96 Å, as depicted in Figure 2. The 2D, 3D binding interactions, and 3D protein positioning of all the investigated compounds towards the aromatase enzyme are shown in the Supplementary Figure S5.

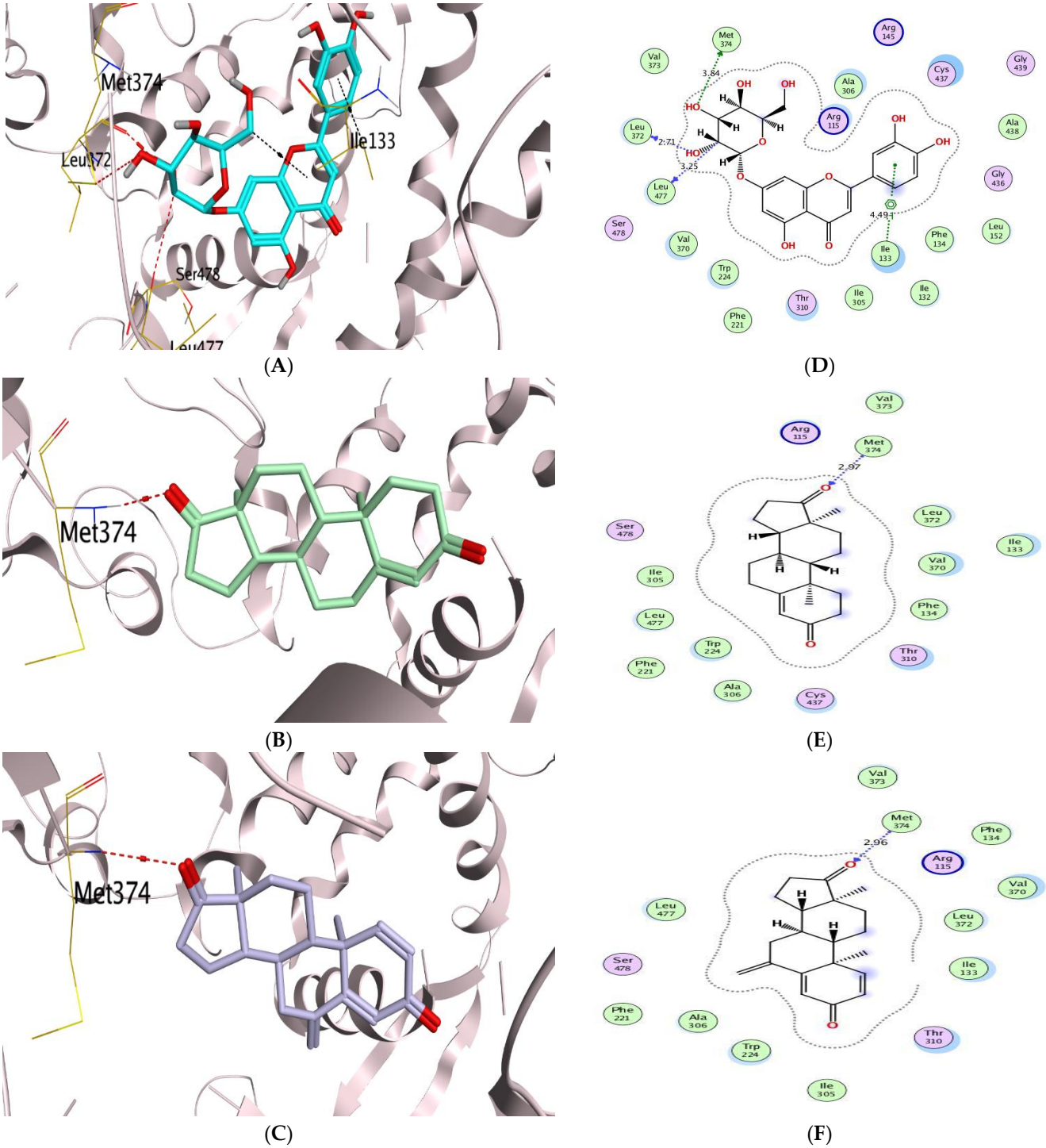

Figure 2. The 3D binding interactions of (**A**) compound (**5**), (**B**) the co-crystallized ligand, (**C**) the reference drug, and the 2D binding interactions of (**D**) compound (**5**), (**E**) the co-crystallized ligand, (**F**) the reference drug at the aromatase enzyme.

Regarding the carbonic anhydrase IX (CA IX) biological target, it was interestingly revealed that compound (**7**) revealed the most binding affinity towards CA IX among the investigated compounds. Additionally, due to their binding to the co-crystallized ligand and reference drug, the amino acids THR200 and THR201 could be considered as crucial amino acids for CA IX inhibition. Consequently, it was disclosed that compound (**7**) could interact with CA IX with a binding score of −8.92 Kcal/mol with an RMSD value of 2.13 Å. Notably, the hydroxyl group of the sugar moiety of compound (**7**) could form an H-bond with THR201 at a distance of 3.22 Å. However, the sulfamoyl moiety of the co-crystallized ligand could form H-bonds with THR200 and THR201 at distances of 3.34, and 3.27 Å, respectively. In addition, the thiophene ring of the co-crystallized ligand could form a pi-H bond with VAL121 at a distance of 4.93 Å. Conversely, the sulfamoyl moiety of the reference drug (Acetazolamide) could form an H-bond with THR200 at a distance of 3.28 Å. Additionally, the thiadiazole ring and the amide moiety of Acetazolamide could form H-bonds with THR201 at distances of 3.22 and 3.29 Å, respectively, as depicted in Figure 3. The 2D, 3D binding interactions, and 3D protein positioning of all investigated compounds towards CA IX are shown in the Supplementary Figure S6.

Regarding the fatty acid synthase (FAS) biological target, it was interestingly revealed that compound (**5**) revealed the most binding affinity towards the FAS among the investigated compounds. Additionally, due to their binding to the the co-crystallized ligand, the amino acids SER2340, TYR2462, and HIS2481 could be treated as key amino acids for FAS inhibition. Consequently, it was disclosed that compound (**5**) could interact with the FAS with a binding score of −6.82 Kcal/mol with an RMSD value of 2.26 Å. Notably, the phenyl ring of compound (**5**) could form two H-bonds with SER2340 at distances of 2.97 and 3.02 Å. In addition, the benzo pyran scaffold of compound (**5**) could form pi-H bonds with PHE2370 and ILE2250 at distances 4.53 and 3.8 Å, respectively. However, the aliphatic chains of the co-crystallized ligand could form pi-H bonds with HIS2481 and TYR2462 at distances of 4.42 and 4.65 Å, respectively. Furthermore, the carbonyl group of the co-crystallized ligand could form an H-bond with SER2340 at a distance of 3.03 Å. Conversely, the phenyl ring of the reference drug ((-)-Epigallocatechin gallate) could form a pi-H bond with HIS2481 at a distance of 3.92 Å as shown in Figure 4. The 2D, 3D binding interactions, and 3D protein positioning of all investigated compounds towards the FAS are shown in the Supplementary Figure S7.

Regarding the Topoisomerase II-DNA complex (TOP II) biological target, it was interestingly revealed that compound (**5**) revealed the most binding affinity towards the TOP II among the investigated compounds. The literature disclosed that the key binding sites of the TOP II comprise the nucleobases; ADE12, GUA13, CYT8, CYT11, and THY9, and the amino acids; ASP479, ARG503, GLN778, and MET782 [53]. Consequently, it was disclosed that compound (**5**) could interact with the TOP II with a binding score of −7.99 Kcal/mol with an RMSD value of 2.15 Å. Notably, the sugar moiety of compound (**5**) could form H-bonds with SER480 and DG at distances of 2.92 and 3.2 Å, respectively. Besides, the benzo pyran scaffold of compound (**5**) could form a pi-H bond with DT at a distance of 3.64 Å, whereas the hydroxyl group of the benzo pyran scaffold of compound (**5**) could form an H-bond with ASP479 at a distance of 2.69 Å. However, the sugar moiety of the co-crystallized ligand could form a pi-H bond with DA and an H-bond with DG at distances of 3.75 and 3.37 Å, respectively. In addition, the dioxane moiety of the co-crystallized ligand could form H-bonds with GLN778 and MET782 at distances of 2.94 and 3.73 Å, respectively. Moreover, the hydroxyl group of the cyclohexyl ring of the co-crystallized ligand could form an H-bond with ASP479 at a distance of 2.7 Å. Conversely, the tetrahydrotetracene scoffold of the reference drug (Doxorubicin) could form H-bonds with ASP479, ARG503, and a pi-H bond with DG13 at distances 3.43, 3.24, and 4.26 Å, respectively. Furthermore, the hydroxyl group on the pyran ring of Doxorubicin could form an H-bond with LYS456 at a distance of 3.29 Å as shown in Figure 5. The 2D, 3D binding interactions, and 3D protein positioning of all investigated compounds towards the TOP II are shown in the Supplementary Figure S8.

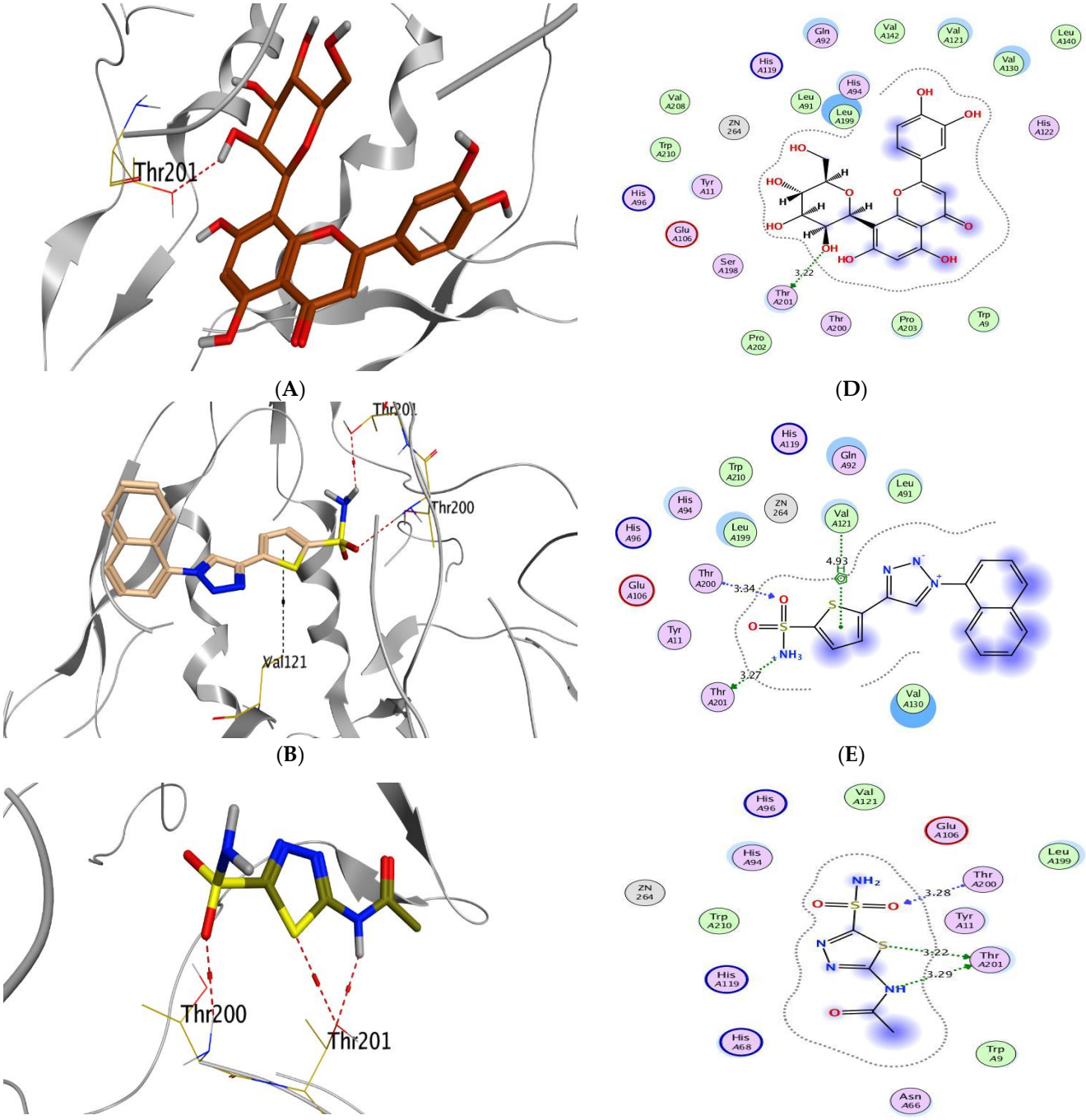

Figure 3. The 3D binding interactions of (**A**) compound **7**, (**B**) the co-crystallized ligand, (**C**) the reference drug, and the 2D binding interactions of (**D**) compound **7**, (**E**) the co-crystallized ligand, (**F**) the reference drug at the **CA IX**.

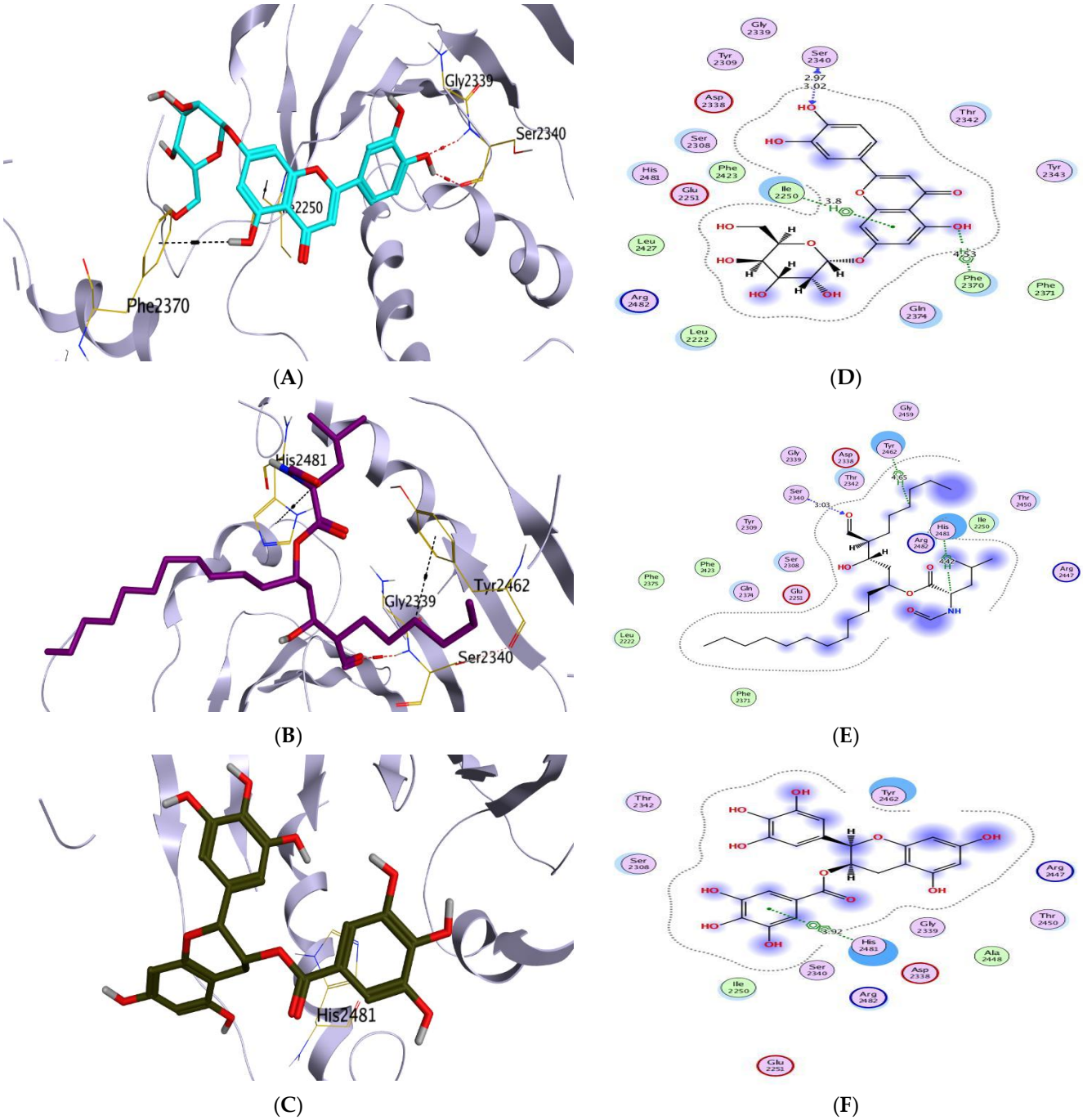

Figure 4. The 3D binding interactions of (**A**) compound **5**, (**B**) the co-crystallized ligand, (**C**) the reference drug, and the 2D binding interactions of (**D**) compound **5**, (**E**) the co-crystallized ligand, (**F**) the reference drug at the **FAS**.

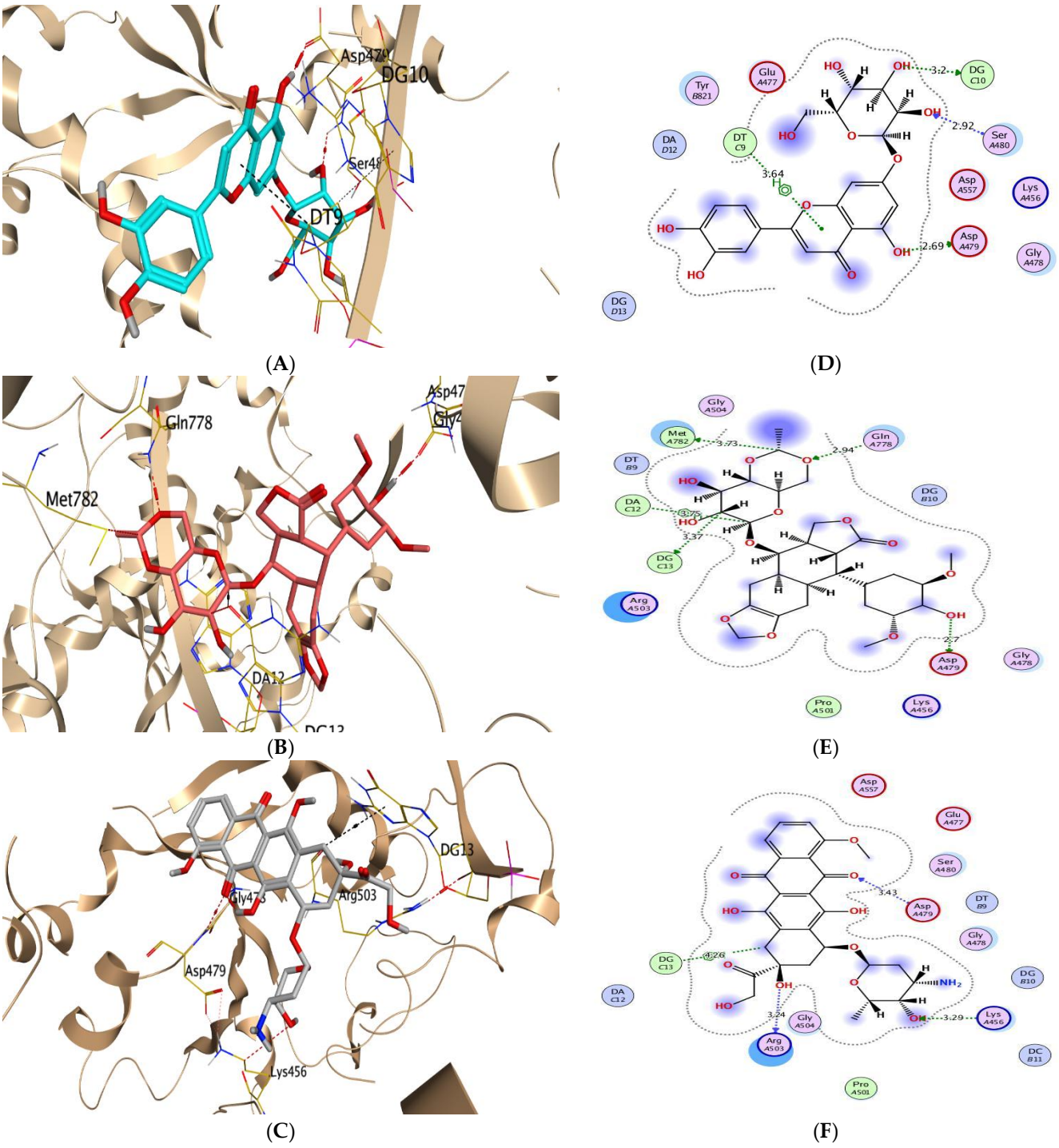

Figure 5. The 3D binding interactions of (**A**) compound (**5**), (**B**) the co-crystallized ligand, (**C**) the reference drug, and the 2D binding interactions of (**D**) compound (**5**), (**E**) the co-crystallized ligand, (**F**) the reference drug at the **TOP II**.

3.3. Prediction of Physicochemical and Pharmacokinetic Properties

The submitted compounds were predicted to display suitable physicochemical and pharmacokinetic properties; logPo/w range 1.0–2.89 and high-water solubility as shown in Table 3 [30]. For high GI absorption and good oral bioavailability for a compound, the physicochemical properties should be within the suitable ranges [54]. The radar charts in Figure 5 displayed the oral bioavailability of our target compounds generated by the SwissADME web tool. This chart has six axes for the six parameters required for oral

bioavailability; flexibility (FLEX), lipophilicity (LIPO), size (SIZE), polarity (POLAR), solubility (INSOLU), and saturation (INSATU) and the pink region in this chart represents the optimal ranges for predicted good oral bioavailability [55]. In Figure 6, the red lines which represent Nepetanudoside C are fully incorporated in the pink area predicting good oral bioavailability. Additionally, the red lines which represent the rest of the compounds are almost entirely incorporated in the pink area predicting acceptable oral bioavailability. Moreover, the SwissADME revealed that geniposide and nepetanudoside C fulfilled Lipinski's rule as one of the major drug likeness characteristics, as such predicting that these compounds may have promising pharmacokinetic properties [56].

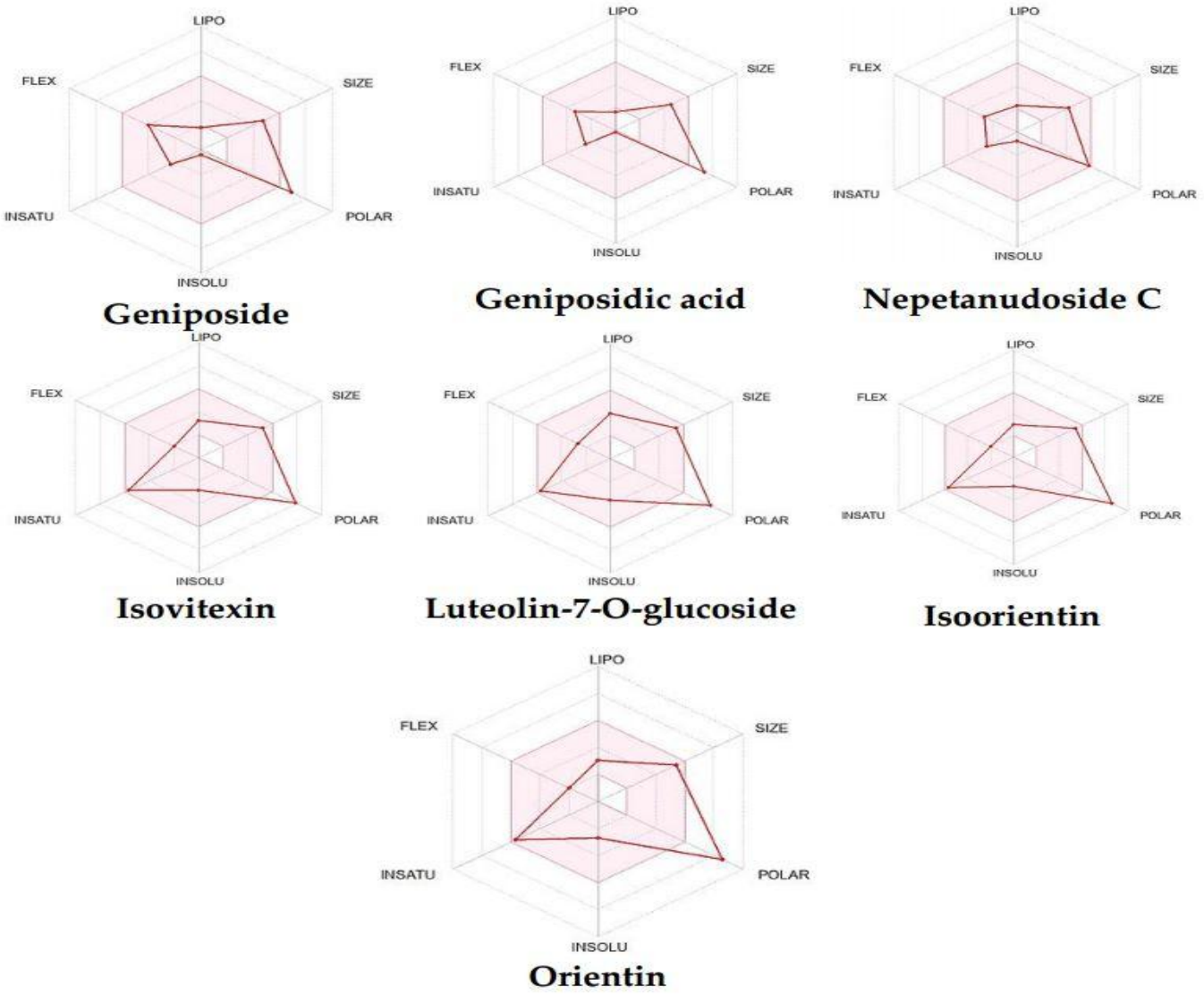

Figure 6. Radar charts for prediction of oral bioavailability generated by the SwissADME web tool.

Table 3. ADMET profile of the target compounds.

Parameter	Geniposide	Geniposidic Acid	Nepetanudoside C	Isovitexin	Luteolin-7-O-glucoside	Isoorientin	Orientin
Physicochemical properties							
Molecular weight	388.14	374.12	342.13	432.11	448.10	448.10	448.10
LogP	2.89	1.31	1.22	1.97	1.99	1.6	1
Rotatable bonds	6	5	4	3	4	3	3
Acceptors	10	10	8	10	11	11	11
Donors	5	6	4	7	7	8	8
Surface area square angstrom ($Å^2$)	155.14	166.14	125.68	181.05	190.28	201.28	201.28
Drug likeness							
Lipinski violations	0	1	0	1	2	2	2
Ghose violations	1	1	1	0	0	1	1
Veber violations	1	1	0	1	1	1	1
Pharmacokinetics							
GI absorption	Low	Low	High	Low	Low	Low	Low
BBB permeant	No	No	No	No	No	No	No
CYP1A2 inhibitor	No	No	No	No	No	No	No
CYP2C19 inhibitor	No	No	No	No	No	No	No
CYP2C9 inhibitor	No	No	No	No	No	No	No
CYP2D6 inhibitor	No	No	No	No	No	No	No
CYP3A4 inhibitor	No	No	No	No	No	No	No
CYP1A2 inhibitor	No	No	No	No	No	No	No
CYP2C19 inhibitor	No	No	No	No	No	No	No
CYP2C9 inhibitor	No	No	No	No	No	No	No

4. Conclusions

The represented work resulted in the isolation, identification, and characterization of seven phytoconstituents that were firstly isolated from the aerial parts of *Pterocephalus frutescens* Hochist. Interestingly, the molecular docking analysis in terms of virtual screening suggested that Luteolin-7-O-glucoside (**5**) was found to exhibit the highest binding affinity among the investigated compounds to aromatase, fatty acid synthase and topoisomerase II-DNA complex, whereas, Orientin (**7**) displayed the highest binding affinity among the investigated compounds to carbonic anhydrase IX. These promising affinities were accomplished through forming strong hydrogen bonds with the catalytic residues, as well as through significant interactions with other receptor-binding residues. Also, the SwissADME online web tool predicted that Luteolin-7-O-glucoside possessed acceptable pharmacokinetics and drug likeness properties. Hence, Luteolin-7-O-glucoside (**5**) and Orientin (**7**) can be considered as lead compounds which can be optimized to develop more potent anticancer agents. We are currently undertaking further studies for the synthesis of novel derivatives and screening the most active compounds for in vitro efficacy against different cell lines and enzymatic assay. In vivo trials in animal models are recommended to take these compounds to the next level of drug discovery.

Supplementary Materials: The following supporting information can be downloaded at: https://www.mdpi.com/article/10.3390/scipharm91010007/s1, Figure S1: (A) 3D diagram and (B) 2D overlay disclosing the superimposition of the native co-crystallized ligand (green), and the redocked co-crystallized ligand (Red) at aromatase enzyme with RMSD value of 1.84 Å for docking program validation; Figure S2: (A) 3D diagram and (B) 2D overlay disclosing the superimposition of the native co-crystallized ligand (green), and the redocked co-crystallized ligand (Red) at CA IV with RMSD value of 1.72 Å for docking program validation; Figure S3: (A) 3D diagram and (B) 2D overlay disclosing the superimposition of the native co-crystallized ligand (green), and the redocked co-crystallized ligand (Red) at FAS with RMSD value of 1.88 Å for docking program validation; Figure S4: (A) 3D diagram and (B) 2D overlay disclosing the superimposition of the native co-crystallized ligand (green), and the redocked co-crystallized ligand (Red) at TOP II with RMSD value of 1.42 Å for

docking program validation; Figure S5: The 2D, 3D, and 3D protein positioning of all investigated compounds at the biological target, aromatase; Figure S6: The 2D, 3D, and 3D protein positioning of all investigated compounds at the biological target, CA IX; Figure S7: the 2D, 3D, and 3D protein positioning of all investigated compounds at the biological target, FAS; Figure S8: the 2D, 3D, and 3D protein positioning of all investigated compounds at the biological target, TOP II.

Author Contributions: Conceptualization, A.A.E.-H. and H.S.A.; methodology, M.S.A.B., A.E.I. and M.M.H.; software, M.M.H., A.A.E. and H.S.A.; validation, M.S.A.B., M.A.D. and A.E.I.; formal analysis, M.M.H. and A.A.E.; investigation, H.S.A.; data curation, M.M.H. and A.A.E.-H.; writing—original draft preparation, H.S.A., A.A.E. and M.M.H.; writing—review and editing, M.M.H., H.S.A. and A.E.I.; visualization, M.S.A.B.; supervision, A.A.E.-H. and S.E.D.; project administration, A.A.E.-H.; funding acquisition, S.E.D. All authors have read and agreed to the published version of the manuscript. All authors have contributed substantially to the work reported.

Funding: This research received no external funding.

Institutional Review Board Statement: Not applicable.

Informed Consent Statement: Not applicable.

Data Availability Statement: All data are available from the corresponding author upon reasonable request.

Conflicts of Interest: The authors declare no conflict of interests.

References

1. Kletter, C.; Kriechbaum, M. *Tibetan Medicinal Plants*; CRC Press: Boca Raton, FL, USA, 2001.
2. El-Hela, A.A.; Hegazy, M.M.; Bakr, M.S.A.; Abbass, H.S. Profiling of antiviral and antioxidant phytochemicals of Pterocephalus frutescens hochist. using high-resolution ultra-performance liquid chromatography/quadrupole time-of-flight mass spectrometer. *Pharmacogn. Mag.* **2020**, *16*, 592–599.
3. Guo, C.; Wu, Y.; Zhu, Y.; Wang, Y.; Tian, L.; Lu, Y.; Han, C.; Zhu, G. In vitro and in vivo antitumor effects of n-butanol extracts of Pterocephalus hookeri on Hep3B cancer cell. *Evid. Based Complement. Altern. Med.* **2015**, *2015*, 159132. [CrossRef] [PubMed]
4. Fahem, A.; Ahmed, A.; Maha, M.; Soltan, A.; Hussein, A.; Zaki, A. Anti-hepatotoxic effect of Pterocephalus sanctus growing in Egypt. *JASRM* **2008**, *3*, 83–87.
5. Vahedi, H.; Nasrabadi, M.; Lari, J.; Halimi, M. Volatile constituents and antimicrobial activities of Pterocephalus canus. *J. Med. Plants Res.* **2011**, *5*, 5646–5648.
6. Wu, Y.-C.; Guo, C.-X.; Zhu, Y.-Z.; Li, Y.-M.; Guo, F.-J.; Zhu, G.-F. Four new bis-iridoids isolated from the traditional Tibetan herb *Pterocephalus hookeri*. *Fitoterapia* **2014**, *98*, 104–109. [CrossRef]
7. Ahmed, F.A.; Shahat, A.A. Flavonoid C-Glycosides from *Pterocephalus Sanctus* Growing in Egypt. *Nat. Prod. Commun.* **2006**, *1*, 1934578X0600100605. [CrossRef]
8. Gülcemal, D.; Masullo, M.; Alankuş-Çalışkan, O.; Karayıldırım, T.; Şenol, S.G.; Piacente, S.; Bedir, E. Monoterpenoid glucoindole alkaloids and iridoids from *Pterocephalus pinardii*. *Magn. Reson. Chem.* **2010**, *48*, 239–243. [CrossRef]
9. Gülcemal, D.; Bedir, E.; Karayıldırım, T.; Milena, M.; Piacente, S.; Şenol, S.; Alankuş-Çalışkan, Ö. Constituents of *Pterocephalus pinardii* Boiss. *Planta Med.* **2009**, *75*, PJ103. [CrossRef]
10. Li, M.-Y.; Deng, H.; Zhao, J.-M.; Dai, D.; Tan, X.-Y. Peroxisome proliferator-activated receptor gamma ligands inhibit cell growth and induce apoptosis in human liver cancer BEL-7402 cells. *World J. Gastroenterol.* **2003**, *9*, 1683–1688. [CrossRef] [PubMed]
11. Smith, J.A.; Maloney, D.J.; Hecht, S.M.; Lannigan, D.A. Structural basis for the activity of the RSK-specific inhibitor, SL0101. *Bioorganic Med. Chem.* **2007**, *15*, 5018–5034. [CrossRef]
12. Gordaliza, M. Natural products as leads to anticancer drugs. *Clin. Transl. Oncol.* **2007**, *9*, 767–776. [CrossRef]
13. Ren, W.; Qiao, Z.; Wang, H.; Zhu, L.; Zhang, L. Flavonoids: Promising anticancer agents. *Med. Res. Rev.* **2003**, *23*, 519–534. [CrossRef] [PubMed]
14. El-Hela, A.A.; Hegazy, M.M.; Abbass, H.S.; Ahmed, A.H.; Bakr, M.S.A.; Elkousy, R.H.; Ibrahim, A.E.; El Deeb, S.; Sayed, O.M.; Gad, E.S. Dinebra retroflexa Herbal Phytotherapy: A Simulation Study Based on Bleomycin-Induced Pulmonary Fibrosis Retraction Potential in Swiss Albino Rats. *Medicina* **2022**, *58*, 1719. [CrossRef]
15. Chumsri, S.; Howes, T.; Bao, T.; Sabnis, G.; Brodie, A. Aromatase, aromatase inhibitors, and breast cancer. *J. Steroid Biochem. Mol. Biol.* **2011**, *125*, 13–22. [CrossRef] [PubMed]
16. Gu, L.; Saha, S.T.; Thomas, J.; Kaur, M. Targeting cellular cholesterol for anticancer therapy. *FEBS J.* **2019**, *286*, 4192–4208. [CrossRef] [PubMed]
17. Almeida, C.F.; Teixeira, N.; Oliveira, A.; Augusto, T.V.; Correia-da-Silva, G.; Ramos, M.J.; Fernandes, P.A.; Amaral, C. Discovery of a multi-target compound for estrogen receptor-positive (ER+) breast cancer: Involvement of aromatase and ERs. *Biochimie* **2021**, *181*, 65–76. [CrossRef]

18. Sanderson, J.T.; Hordijk, J.; Denison, M.S.; Springsteel, M.F.; Nantz, M.H.; Berg, M.V.D. Induction and Inhibition of Aromatase (CYP19) Activity by Natural and Synthetic Flavonoid Compounds in H295R Human Adrenocortical Carcinoma Cells. *Toxicol. Sci.* **2004**, *82*, 70–79. [CrossRef]
19. Kuhajda, F.P.; Pizer, E.S.; Li, J.N.; Mani, N.S.; Frehywot, G.L.; Townsend, C.A. Synthesis and antitumor activity of an inhibitor of fatty acid synthase. *Proc. Natl. Acad. Sci. USA* **2000**, *97*, 3450–3454. [CrossRef]
20. Fhu, C.W.; Ali, A. Fatty Acid Synthase: An Emerging Target in Cancer. *Molecules* **2020**, *25*, 3935. [CrossRef]
21. Brusselmans, K.; Vrolix, R.; Verhoeven, G.; Swinnen, J.V. Induction of Cancer Cell Apoptosis by Flavonoids Is Associated with Their Ability to Inhibit Fatty Acid Synthase Activity. *J. Biol. Chem.* **2005**, *280*, 5636–5645. [CrossRef] [PubMed]
22. Hegazy, M.M.; Afifi, W.M.; Metwaly, A.M.; Radwan, M.M.; Abd-Elraouf, M.; Mehany, A.B.M.; Ahmed, E.; Enany, S.; Ezzeldin, S.; Ibrahim, A.E.; et al. Antitrypanosomal, Antitopoisomerase-I, and Cytotoxic Biological Evaluation of Some African Plants Belonging to Crassulaceae; Chemical Profiling of Extract Using UHPLC/QTOF-MS/MS. *Molecules* **2022**, *27*, 8809. [CrossRef] [PubMed]
23. Bjornsti, M.-A.; Kaufmann, S.H. Topoisomerases and cancer chemotherapy: Recent advances and unanswered questions. *F1000Research* **2019**, *8*, 1704. [CrossRef] [PubMed]
24. Han, S.; Lim, K.S.; Blackburn, B.J.; Yun, J.; Putnam, C.W.; Bull, D.A.; Won, Y.-W. The Potential of Topoisomerase Inhibitor-Based Antibody–Drug Conjugates. *Pharmaceutics* **2022**, *14*, 1707. [PubMed]
25. Okura, A.; Arakawa, H.; Oka, H.; Yoshinari, T.; Monden, Y. Effect of genistein on topoisomerase activity and on the growth of [VAL 12]Ha-ras-transformed NIH 3T3 cells. *Biochem. Biophys. Res. Commun.* **1988**, *157*, 183–189. [CrossRef]
26. Hevener, K.; Verstak, T.A.; Lutat, K.E.; Riggsbee, D.L.; Mooney, J.W. Recent developments in topoisomerase-targeted cancer chemotherapy. *Acta Pharm. Sin. B* **2018**, *8*, 844–861. [CrossRef]
27. Pastorekova, S.; Gillies, R.J. The role of carbonic anhydrase IX in cancer development: Links to hypoxia, acidosis, and beyond. *Cancer Metastasis Rev.* **2019**, *38*, 65–77. [CrossRef]
28. Saghafi, T.; Taheri, R.A.; Parkkila, S.; Emameh, R.Z. Phytochemicals as Modulators of Long Non-Coding RNAs and Inhibitors of Cancer-Related Carbonic Anhydrases. *Int. J. Mol. Sci.* **2019**, *20*, 2939. [CrossRef]
29. McDonald, P.C.; Chafe, S.C.; Supuran, C.T.; Dedhar, S. Cancer Therapeutic Targeting of Hypoxia Induced Carbonic Anhydrase IX: From Bench to Bedside. *Cancers* **2022**, *14*, 3297. [CrossRef]
30. Daina, A.; Michielin, O.; Zoete, V. SwissADME: A free web tool to evaluate pharmacokinetics, drug-likeness and medicinal chemistry friendliness of small molecules. *Sci. Rep.* **2017**, *7*, 42717. [CrossRef]
31. Elmaaty, A.A.; Darwish, K.M.; Khattab, M.; Elhady, S.S.; Salah, M.; Hamed, M.I.; Al-Karmalawy, A.A.; Saleh, M.M. In a search for potential drug candidates for combating COVID-19: Computational study revealed salvianolic acid B as a potential therapeutic targeting 3CLpro and spike proteins. *J. Biomol. Struct. Dyn.* **2021**, *40*, 8866–8893. [CrossRef]
32. Elmaaty, A.A.; Alnajjar, R.; Hamed, M.I.; Khattab, M.; Khalifa, M.M.; Al-Karmalawy, A.A. Revisiting activity of some glucocorticoids as a potential inhibitor of SARS-CoV-2 main protease: Theoretical study. *RSC Adv.* **2021**, *11*, 10027–10042. [CrossRef] [PubMed]
33. Elmaaty, A.A.; Hamed, M.I.; Ismail, M.I.; Elkaeed, E.B.; Abulkhair, H.S.; Khattab, M.; Al-Karmalawy, A.A. Computational insights on the potential of some NSAIDs for treating COVID-19: Priority set and lead optimization. *Molecules* **2021**, *26*, 3772. [CrossRef]
34. Hamed, M.I.; Darwish, K.M.; Soltane, R.; Chrouda, A.; Mostafa, A.; Shama, N.M.A.; Elhady, S.S.; Abulkhair, H.S.; Khodir, A.E.; Elmaaty, A.A. β-Blockers bearing hydroxyethylamine and hydroxyethylene as potential SARS-CoV-2 Mpro inhibitors: Rational based design, in silico, in vitro, and SAR studies for lead optimization. *RSC Adv.* **2021**, *11*, 35536–35558. [CrossRef] [PubMed]
35. Elmaaty, A.A.; Darwish, K.M.; Chrouda, A.; Boseila, A.A.; Tantawy, M.A.; Elhady, S.S.; Shaik, A.B.; Mustafa, M.; Al-Karmalawy, A.A. In Silico and In Vitro Studies for Benzimidazole Anthelmintics Repurposing as VEGFR-2 Antagonists: Novel Mebendazole-Loaded Mixed Micelles with Enhanced Dissolution and Anticancer Activity. *ACS Omega* **2021**, *7*, 875–899. [CrossRef]
36. Elebeedy, D.; Badawy, I.; Elmaaty, A.A.; Saleh, M.M.; Kandeil, A.; Ghanem, A.; Kutkat, O.; Alnajjar, R.; El Maksoud, A.I.A.; Al-Karmalawy, A.A. In vitro and computational insights revealing the potential inhibitory effect of Tanshinone IIA against influenza A virus. *Comput. Biol. Med.* **2021**, *141*, 105149. [CrossRef] [PubMed]
37. Hammoud, M.M.; Nageeb, A.S.; Morsi, M.A.; Gomaa, E.A.; Elmaaty, A.A.; Al-Karmalawy, A.A. Design, synthesis, biological evaluation, and SAR studies of novel cyclopentaquinoline derivatives as DNA intercalators, topoisomerase II inhibitors, and apoptotic inducers. *New J. Chem.* **2022**, *46*, 11422–11436. [CrossRef]
38. Hammoud, M.M.; Elmaaty, A.A.; Nafie, M.S.; Abdel-Motaal, M.; Mohamed, N.S.; Tantawy, M.A.; Belal, A.; Alnajjar, R.; Eldehna, W.M.; Al-Karmalawy, A.A. Design and synthesis of novel benzoazoninone derivatives as potential CBSIs and apoptotic inducers: In Vitro, in Vivo, molecular docking, molecular dynamics, and SAR studies. *Bioorganic Chem.* **2022**, *127*, 105995. [CrossRef] [PubMed]
39. Ghosh, D.; Egbuta, C.; Lo, J. Testosterone complex and non-steroidal ligands of human aromatase. *J. Steroid Biochem. Mol. Biol.* **2018**, *181*, 11–19. [CrossRef]
40. Leitans, J.; Kazaks, A.; Balode, A.; Ivanova, J.; Zalubovskis, R.; Supuran, C.T.; Tars, K. Efficient Expression and Crystallization System of Cancer-Associated Carbonic Anhydrase Isoform IX. *J. Med. Chem.* **2015**, *58*, 9004–9009. [CrossRef]
41. Pemble, C.W.; Johnson, L.C.; Kridel, S.J.; Lowther, W.T. Crystal structure of the thioesterase domain of human fatty acid synthase inhibited by Orlistat. *Nat. Struct. Mol. Biol.* **2007**, *14*, 704–709. [CrossRef]

42. Wu, C.-C.; Li, T.-K.; Farh, L.; Lin, L.-Y.; Lin, T.-S.; Yu, Y.-J.; Yen, T.-J.; Chiang, C.-W.; Chan, N.-L. Structural Basis of Type II Topoisomerase Inhibition by the Anticancer Drug Etoposide. *Science* **2011**, *333*, 459–462. [CrossRef] [PubMed]
43. Güvenalp, Z.; Kilic, N.; Kazaz, C.; Kaya, Y.; Demirezer, L.Ö. Chemical constituents of Galium tortumense. *Turk. J. Chem.* **2006**, *30*, 515–523.
44. Takeda, Y.; Morimoto, Y.; Matsumoto, T.; Honda, G.; Tabata, M.; Fujita, T.; Otsuka, H.; Sezik, E.; Yesilada, E. Nepetanudoside, an iridoid glucoside with an unusual stereostructure from Nepeta nuda ssp. albiflora. *J. Nat. Prod.* **1995**, *58*, 1217–1221. [CrossRef]
45. Huang, D.; Guo, W.; Gao, J.; Chen, J.; Olatunji, J.O. Clinacanthus nutans (Burm. f.) Lindau Ethanol Extract Inhibits Hepatoma in Mice through Upregulation of the Immune Response. *Molecules* **2015**, *20*, 17405–17428. [CrossRef] [PubMed]
46. de Oliveira, D.; Siqueira, E.P.; Nunes, Y.R.F.; Cota, B.B. Flavonoids from leaves of Mauritia flexuosa. *Rev. Bras. de Farm.* **2013**, *23*, 614–620. [CrossRef]
47. Chiruvella, K.K.; Mohammed, A.; Dampuri, G.; Ghanta, R.G.; Raghavan, S.C. Phytochemical and Antimicrobial Studies of Methyl Angolensate and Luteolin-7-O-glucoside Isolated from Callus Cultures of Soymida febrifuga. *IJBS* **2007**, *3*, 269–278.
48. El-Demerdash, A.; Al-Karmalawy, A.A.; Abdel-Aziz, T.M.; Elhady, S.S.; Darwish, K.M.; Hassan, A.H.E. Investigating the structure–activity relationship of marine natural polyketides as promising SARS-CoV-2 main protease inhibitors. *RSC Adv.* **2021**, *11*, 31339–31363. [CrossRef] [PubMed]
49. Elebeedy, D.; Elkhatib, W.F.; Kandeil, A.; Ghanem, A.; Kutkat, O.; Alnajjar, R.; Saleh, M.A.; Abd El Maksoud, A.I.; Badawy, I.; Al-Karmalawy, A.A. Anti-SARS-CoV-2 activities of tanshinone IIA, carnosic acid, rosmarinic acid, salvianolic acid, baicalein, and glycyrrhetinic acid between computational and in vitro insights. *RSC Adv.* **2021**, *11*, 29267–29286. [CrossRef] [PubMed]
50. Khattab, M.; Al-Karmalawy, A.A. Computational repurposing of benzimidazole anthelmintic drugs as potential colchicine binding site inhibitors. *Futur. Med. Chem.* **2021**, *13*, 1623–1638. [CrossRef] [PubMed]
51. Ghanem, A.; Al-Karmalawy, A.A.; El Maksoud, A.I.A.; Hanafy, S.M.; Emara, H.A.; Saleh, R.M.; Elshal, M.F. Rumex Vesicarius L. extract improves the efficacy of doxorubicin in triple-negative breast cancer through inhibiting Bcl2, mTOR, JNK1 and augmenting p21 expression. *Informatics Med. Unlocked* **2022**, *29*, 100869. [CrossRef]
52. Asmari, M.; Waqas, M.; Ibrahim, A.E.; Halim, S.A.; Khan, A.; Al-Harrasi, A.; Wätzig, H.; El Deeb, S. Microscale Thermophoresis and Molecular Modelling to Explore the Chelating Drug Transportation in the Milk to Infant. *Molecules* **2022**, *27*, 4604. [CrossRef] [PubMed]
53. El-Naggar, A.M.; Abou-El-Regal, M.M.; El-Metwally, S.A.; Sherbiny, F.F.; Eissa, I.H. Synthesis, characterization and molecular docking studies of thiouracil derivatives as potent thymidylate synthase inhibitors and potential anticancer agents. *Mol. Divers.* **2017**, *21*, 967–983. [CrossRef] [PubMed]
54. Gomaa, E.; El Deeb, S.; Ibrahim, A.E.; Faisal, M.M. Bimodal Release Two-In-One Clonazepam Matrix Lozenge Tablets for Managing Anxiety-Related Disorders: Formulation, Optimization and In Vivo Evaluation. *Sci. Pharm.* **2022**, *90*, 43. [CrossRef]
55. Daina, A.; Michielin, O.; Zoete, V. iLOGP: A Simple, Robust, and Efficient Description of n-Octanol/Water Partition Coefficient for Drug Design Using the GB/SA Approach. *J. Chem. Inf. Model.* **2014**, *54*, 3284–3301. [CrossRef]
56. Lipinski, C.A.; Lombardo, F.; Dominy, B.W.; Feeney, P.J. Experimental and computational approaches to estimate solubility and permeability in drug discovery and development settings. *Adv. Drug Deliv. Rev.* **2012**, *64*, 4–17. [CrossRef]